Equilibrium current in a Weyl semimetal–superconductor heterostructure

K. A. Madsen, P. W. Brouwer, and M. Breitkreiz*
Dahlem Center for Complex Quantum Systems and Fachbereich Physik, Freie Universität Berlin, 14195 Berlin, Germany

(Received 16 April 2021; revised 18 June 2021; accepted 22 June 2021; published 6 July 2021)

A heterostructure consisting of a magnetic Weyl semimetal and a conventional superconductor exhibits an equilibrium current parallel to the superconductor interface and perpendicular to the magnetization. Analyzing a minimal model, which as a function of parameters may be in a trivial magnetic insulator phase, a Weyl semimetal phase, or a three-dimensional weak Chern insulator phase, we find that the equilibrium current is sensitive to the presence of surface states, such as the topological Fermi-arc states of the Weyl semimetal or the chiral surface states of the weak Chern insulator. While there is a nonzero equilibrium current in all three phases, the appearance of the surface states in the topological regime leads to a reversal of the direction of the current, compared to the current direction for the trivial magnetic insulator phase. We discuss the interpretation of the surface-state contribution to the equilibrium current as a real-space realization of the superconductivity-enabled equilibrium chiral magnetic effect of a single chirality, predicted to occur in bulk Weyl superconductors.

DOI: 10.1103/PhysRevB.104.035109

I. INTRODUCTION

A Weyl semimetal is a three-dimensional crystal with topologically protected nodal points in the band structure [1–3]. The nodes have a well-defined chirality and they appear in pairs, such that in total the sum of the chiralities vanishes [4]. One manifestation of chiral Weyl nodes and the associated chiral anomaly in crystals is the existence of topologically protected surface states, which connect the projections of two Weyl nodes of opposite chirality on the surface band structure, in the form of two "Fermi arcs" located at opposite surfaces of the Weyl semimetal and moving in opposite directions. Another manifestation is the chiral magnetic effect—an external-magnetic-field induced current of Weyl Fermions directed parallel or antiparallel to the magnetic field depending on the chirality—which leads to unusual nonequilibrium transport properties of the crystal [5–9]. In equilibrium the chiral anomaly usually remains hidden since the chiral currents must compensate each other, in agreement with general band-theoretic considerations [10].

As was shown by O'Brien, Beenakker, and Adagideli [11] (see also Ref. [12]), there is, however, a way to circumvent the compensation of chiral anomalies in equilibrium with the help of superconductivity. This is most easily seen in a minimal model of a magnetic Weyl semimetal with two Weyl nodes of opposite chirality and a superconducting s-wave pair potential. If the pair momentum is tuned to the momentum of one of the two Weyl nodes via a flux or a supercurrent bias, superconductivity is induced there and the Weyl node is gapped out, while the node of opposite chirality is left mostly unaffected. In an applied magnetic field, this unaffected chirality gives rise to an equilibrium current, as the opposite chirality is no longer available to carry the compensating current. Unfortunately, making a Weyl semimetal superconducting [13–16] meets the difficulty of a vanishing density of states at the Weyl nodes, which suppresses the critical temperature. Another obstacle, specifically in the case of a magnetic Weyl semimetal considered in this work, is the competition with magnetism.

An alternative route to achieve superconducting phases in Weyl semimetals is to make use of the proximity-induced superconductivity in heterostructures by combining an otherwise nonsuperconducting Weyl semimetal (N) and a conventional superconductor (S) [17–20]. One prominent type of such heterostructures is the Josephson junction (SNS-heterostructure), which has been extensively studied theoretically exploring the influence of various types of superconducting pairing mechanisms [21–35] and has also been realized experimentally [19,36–40]. Other examples of similar heterostructures are NS-type [17,20,41–51], and NSN-type [52–56] heterostructures.

While most of these studies investigate equilibrium currents that flow perpendicular to the superconductor–Weyl-semimetal interface, in this article we theoretically investigate the equilibrium current in a bilayer consisting of a Weyl semimetal and a single superconductor (SN bilayer), as illustrated in Fig. 1, for which the equilibrium current flows parallel to the interface. We consider a magnetic Weyl semimetal and a conventional s-wave superconductor, both are microscopically inversion-symmetric, so that inversion symmetry is broken only by the interface. To allow for a comparison between different phases, we consider a model for the normal region which, as a function of parameters, may be in a trivial magnetic insulator phase, Weyl semimetal phase, or a (three-dimensional) weak Chern insulator phase. We find a significant contribution to the equilibrium current from surface states (Fermi arcs in case of a Weyl semimetal, chiral surface states for the weak Chern insulator), which differs in sign and magnitude from the interfacial current of a trivial insulator [57]. Although our minimal model shows

*breitkr@physik.fu-berlin.de

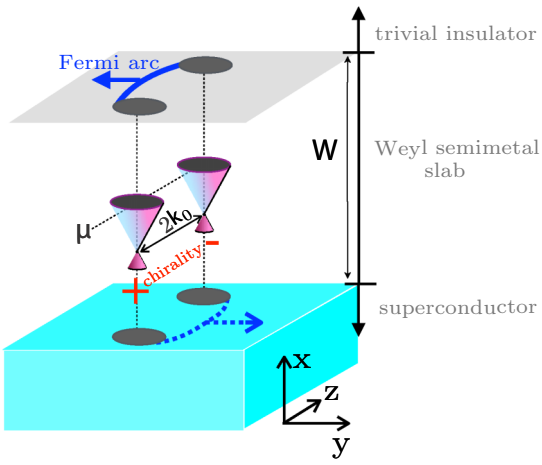

FIG. 1. Mixed momentum/real-space illustration of the SN heterostructure considered in this article. It consists of a Weyl semimetal slab of a finite width W with two Weyl nodes separated along the k_z axis and counterpropagating Fermi arcs on the top (solid blue) and bottom (dotted blue) surfaces. The Weyl semimetal slab borders on a superconductor (light blue) at the bottom surface and it is capped by a trivial insulator at the top surface. Because of this built-in spatial asymmetry of the heterostructure, the superconducting proximity effect acts asymmetrically on the two Fermi arcs.

a clear signature at the onset of the topological regime, the magnitude of the equilibrium current is nonuniversal because for an inversion-symmetric Weyl semimetal the proximity superconductivity pairs electrons in the topological low-energy band with electrons in a nontopological high-energy band—an effect known as "chirality blockade" [22]. For the minimal model we can isolate the singular contribution to the current from the Fermi-arc surface states by comparing equilibrium currents in a finite-width slab for a chemical potential inside and outside the finite-size gap of the Fermi-arc states at the Weyl node.

The contribution of topological surface states can be interpreted as the result of an effective charge renormalization of the chiral surface modes at the *SN* interface [58], which leads to a disbalance with the counterpropagating surface modes of the opposite surface and results in a finite current. In this way, the idea of bulk superconductivity acting asymmetrically on chiral states in momentum space [11,12] is transferred to proximitized superconductivity acting asymmetrically on chiral states in real space. In the first case the equilibrium current is carried by the disbalanced chiral Weyl Fermions in an external magnetic field, in the second by the disbalanced chiral surface states at zero external magnetic field.

This article is structured as follows. After introducing the minimal model for the *SN* heterostructure in Sec. II, we calculate and discuss the equilibrium current in Sec. III. We conclude in Sec. IV.

II. MODEL

We consider a bilayer consisting of a superconductor (S) and a normal region (N) of width W. We choose coordinates such that the x axis is perpendicular to the superconductor interface and the superconductor interface is at $x = 0$. The normal region corresponds to $0 < x < W$.

Depending on the parameters in our model Hamiltonian, the normal region is a topologically trivial magnetic insulator, a magnetic Weyl semimetal, or a three-dimensional weak Chern insulator. At $x = W$ the normal region layer is capped by a nonmagnetic trivial insulator. Below, we give lattice models for the Weyl semimetal, the superconductor, and the trivial insulator. To keep the notation simple, the lattice constant and $\hbar$ are set to unity.

A. Normal region

We model the normal region with the four-band Hamiltonian

$$H^{(\mathrm{W})}(\boldsymbol{k}) = t\tau_3(\sigma_1 \sin k_x + \sigma_2 \sin k_y) + m(\boldsymbol{k})\tau_1\sigma_0 + \beta\tau_0\sigma_3 - \mu\tau_0\sigma_0, \quad (1)$$

with

$$m(\boldsymbol{k}) = m_0 + t'(2 - \cos k_x - \cos k_y) + t'_z(1 - \cos k_z), \quad (2)$$

where the σ_i and τ_i, $i = 0, 1, 2, 3$ are Pauli matrices corresponding to spin and orbital degrees of freedom, respectively. (These include the identity matrices σ_0 and τ_0.) Furthermore, μ is the chemical potential; t, t', and t'_z are hopping parameters; m_0 an orbital-selective on-site potential; and β the exchange field, which is directed in the z direction. For definiteness, all of these parameters are assumed to be positive. The Hamiltonian, shown in Eq. (1), satisfies inversion symmetry

$$H^{(\mathrm{W})}(\boldsymbol{k}) = \tau_1 H^{(\mathrm{W})}(-\boldsymbol{k})\tau_1, \quad (3)$$

whereas time-reversal symmetry is broken by the exchange field. (Time-reversal symmetry is represented as $\sigma_2 K$, where K is complex conjugation.) At zero chemical potential μ, the Hamiltonian, see Eq. (1), also satisfies a mirror antisymmetry

$$H^{(\mathrm{W})}_{\mu=0}(k_x, k_y, k_z) = -\sigma_2\tau_3 H^{(\mathrm{W})}_{\mu=0}(k_x, -k_y, k_z)\sigma_2\tau_3. \quad (4)$$

The Hamiltonian, given in Eq. (1), resembles minimal models motivated by materials of the Bi_2Se_3 family [10], where, however, for simplicity we omitted a term proportional to $\tau_3\sigma_3 \sin k_z$. [Such a term does not significantly alter the topological phases that we are going to study, but its absence makes the analysis more transparent. A term $\propto \tau_3\sigma_3 \sin k_z$ preserves the inversion symmetry, Eq. (3), and the mirror antisymmetry, Eq. (4), at $\mu = 0$. We verified that our conclusions remain valid if we include this term.]

The eigenvalues of the Hamiltonian, Eq. (1), can easily be calculated in closed form. For each momentum $\boldsymbol{k}$ there are four eigenvalues, labeled $\varepsilon_{\pm,\pm}$,

$$\varepsilon_{\pm,\pm}(\boldsymbol{k}) = -\mu \pm \sqrt{t^2(\sin^2 k_x + \sin^2 k_y) + (m(\boldsymbol{k}) \pm \beta)^2}. \quad (5)$$

The two bands with energy eigenvalues $\varepsilon_{\pm,+}(\boldsymbol{k})$ are completely gapped. The other two bands, which have energy eigenvalues $\varepsilon_{\pm,-}(\boldsymbol{k})$, may also be gapped or feature two Weyl nodes, depending on the value of the exchange field β. The Weyl-semimetal phase is found for

$$m_0 < \beta < m_0 + 2t'_z. \quad (6)$$

In this case, two Weyl nodes exist at $\boldsymbol{k} = (0, 0, \pm k_0)$, with

$$k_0 = 2 \arcsin \sqrt{\frac{\beta - m_0}{2t_z'}}, \quad m_0 < \beta < m_0 + 2t_z'. \tag{7}$$

For $\beta \downarrow m_0$, one has $k_0 \to 0$: The two Weyl nodes merge at $k_z = 0$ and gap out for $\beta < m_0$. Hence, for

$$0 < \beta < m_0 \tag{8}$$

the system becomes a trivial insulator, which for a finite exchange field $\beta > 0$ is magnetic. For $\beta \uparrow m_0 + 2t_z'$, one has $k_0 \to \pi$, and the Weyl nodes merge and gap out at the Brillouin zone boundary. For

$$\beta > m_0 + 2t_z' \tag{9}$$

the system thus becomes a weak Chern insulator [59,60], which has open surface-state contours extending over the whole Brillouin zone.

To prepare for the description of superconductor heterostructures using the Bogoliubov–de Gennes (BdG) formalism, we double the degrees of freedom by introducing holes with Hamiltonian $-\sigma_2 H^{(\mathrm{W})}(-\boldsymbol{k})^* \sigma_2$. The resulting Bogoliubov–de Gennes Hamiltonian

$$\mathcal{H}^{(\mathrm{W})} = \begin{pmatrix} H^{(\mathrm{W})} & 0 \\ 0 & -\sigma_2 H^{(\mathrm{W})}(-\boldsymbol{k})^* \sigma_2 \end{pmatrix} \tag{10}$$

has particle-hole symmetry

$$\mathcal{H}(\boldsymbol{k}) = -\nu_2 \sigma_2 \mathcal{H}(-\boldsymbol{k})^* \nu_2 \sigma_2, \tag{11}$$

where Pauli matrices ν_j, $j = 0, 1, 2, 3$, represent the particle-hole degree of freedom.

B. Heterostructure

The normal region at $0 < x < W$ is embedded between a superconductor for $x < 0$ and a trivial insulator for $x > W$, both of which we model by semi-infinite systems in the following way: The lattice Hamiltonians for the superconductor (S) and trivial insulator (I) in the Bogoliubov–de Gennes formulation are

$$\mathcal{H}^{(\mathrm{S})}(\boldsymbol{k}) = t \nu_3 \tau_3 \sigma_1 \sin k_x + \Delta \nu_1 \tau_0 \sigma_0, \tag{12}$$

$$\mathcal{H}^{(\mathrm{I})}(\boldsymbol{k}) = t \nu_3 \tau_3 \sigma_1 \sin k_x + m^{(\mathrm{I})} \nu_3 \tau_1 \sigma_0, \tag{13}$$

where $\Delta > 0$ is the superconducting order parameter and $m^{(\mathrm{I})} \to \infty$ the mass gap in the insulating region. Both the superconductor and the insulator satisfy inversion symmetry

$$\mathcal{H}^{(\mathrm{S,I})}(\boldsymbol{k}) = \tau_1 \mathcal{H}^{(\mathrm{S,I})}(-\boldsymbol{k}) \tau_1, \tag{14}$$

characteristic of superconducting order with even inversion parity, and time-reversal symmetry

$$\mathcal{H}^{(\mathrm{S,I})}(\boldsymbol{k}) = \sigma_2 \mathcal{H}^{(\mathrm{S,I})}(-\boldsymbol{k})^* \sigma_2. \tag{15}$$

To describe the heterostructure with an x-dependent Hamiltonian, we replace k_x by $-i\partial_x$ and linearize the Hamiltonians $\mathcal{H}^{(\mathrm{W})}$, $\mathcal{H}^{(\mathrm{S})}$, and $\mathcal{H}^{(\mathrm{I})}$ in k_x. In this way, we obtain the Hamiltonian

$$\mathcal{H} = -it \nu_3 \tau_3 \sigma_1 \partial_x + \mathcal{M}(x), \tag{16}$$

where

$$\mathcal{M}(x) = \mathcal{M}^{(\mathrm{S})} \equiv \Delta \nu_1 \sigma_0 \tag{17a}$$

for $x < 0$,

$$\mathcal{M}(x) = \mathcal{M}^{(\mathrm{W})} \equiv t \nu_3 \tau_3 \sigma_2 \sin k_y + m(k_y, k_z) \nu_3 \tau_1 \sigma_0 + \beta \nu_0 \sigma_3 - \mu \nu_3 \sigma_0 \tag{17b}$$

for $0 < x < W$, and

$$\mathcal{M}(x) = \mathcal{M}^{(\mathrm{I})} \equiv m^{(\mathrm{I})} \nu_3 \tau_1 \sigma_0 \tag{17c}$$

for $x > W$, respectively. Here

$$m(k_y, k_z) = m_0 + t'(1 - \cos k_y) + t_z'(1 - \cos k_z) \tag{18}$$

is the linearized mass term in the normal region.

C. Block diagonalization, chirality, Fermi arcs

A unitary transformation can be used to bring the Hamiltonian to a block-diagonal form. Labeling the two blocks by the parameter $\tau = \pm 1$, the transformation reads

$$\mathcal{H}_\tau = [U \mathcal{H} U^\dagger]_\tau, \quad U = e^{i(\pi/4)\nu_0 \tau_2 \sigma_3}. \tag{19}$$

The transformation acts nontrivially only on the mass term, which transforms as

$$[U \nu_3 \tau_1 \sigma_0 U^\dagger]_\tau = \tau \nu_3 \sigma_3, \tag{20}$$

while the transformation of the other terms simply replaces τ_3 by τ. After the unitary transformation from Eq. (19) the diagonal blocks of the Hamiltonian, Eq. (16) then read

$$\mathcal{H}_\tau = -it\tau \nu_3 \sigma_1 \partial_x + \mathcal{M}_\tau(x), \tag{21}$$

with $\mathcal{M}_\tau(x) = \mathcal{M}^{(\mathrm{S})}$, given by Eq. (17a), for $x < 0$, $\mathcal{M}(x) = \mathcal{M}_\tau^{(\mathrm{W})}$,

$$\mathcal{M}_\tau^{(\mathrm{W})} = t\tau \nu_3 \sigma_2 \sin k_y + m(k_y, k_z) \tau \mu_3 \sigma_3 - \mu \nu_3 \sigma_0 + \beta \nu_0 \sigma_3 \tag{22}$$

for $0 < x < W$, and $\mathcal{M}(x) = \mathcal{M}^{(\mathrm{I})}$,

$$\mathcal{M}_\tau^{(\mathrm{I})} = m^{(\mathrm{I})} \tau \nu_3 \sigma_3 \tag{23}$$

for $x > W$. In the transformed basis, inversion, time-reversal, particle-hole conjugation, and the mirror antisymmetry shown in Eq. (4) are represented as $\tau_3 \sigma_3$, $\tau_2 \sigma_1 K$, $\nu_2 \tau_2 \sigma_1 K$, and $\sigma_2 \tau_3$, respectively.

After the unitary transformation, the Weyl nodes are found in the blocks $\tau = -1$ for electrons and $\tau = +1$ for holes, respectively. Expanding $\mathcal{H}_\tau^{(\mathrm{W})}$ around the Weyl nodes in the form $\sum_i v_i \sigma_i (k_i - K_i)$, where K_i is the node position, we can identify the chirality $\chi = \mathrm{sgn}(v_1 v_2 v_3)$. For our convention that all model parameters are positive, $\chi = \mp$ for the node at $k_z = \pm k_0$ for both electrons and holes, as indicated for electrons in Fig. 1.

To find Fermi-arc surface states at the interface with the trivial insulator at $x = W$, we consider electron and hole

eigenstates of the insulator that decay for $x > W$, taken at $x = W$,

$$\psi_{\mathrm{e/h}}(W) = a_{\mathrm{e/h}}\begin{pmatrix}1\\ i\end{pmatrix}, \tag{24}$$

with normalization coefficients $a_{\mathrm{e/h}}$ that have to be determined separately. For the normal region $x < W$ we use the ansatz

$$\psi_{\mathrm{e/h}}(x) = a_{\mathrm{e/h}}\begin{pmatrix}1\\ i\end{pmatrix}e^{\alpha(x-W)}. \tag{25}$$

The decay coefficient $\alpha > 0$ and the energy ε can be found by insertion of the ansatz of Eq. (25) into the Bogoliubov–de Gennes equation

$$\left[\mathcal{H}_\tau^{(\mathrm{W})} - \varepsilon\right]\begin{pmatrix}\psi_e(x)\\ \psi_h(x)\end{pmatrix} = 0. \tag{26}$$

For $\tau = -1$ we find an electron-like solution with $\alpha = \beta - m(k_y, k_z)$ and energy

$$\varepsilon_{\mathrm{e}}(k_y, k_z) = -t\sin k_y - \mu. \tag{27}$$

For $\tau = +1$, the solution is hole-like and has energy

$$\varepsilon_{\mathrm{h}}(k_y, k_z) = -t\sin k_y + \mu. \tag{28}$$

Both solutions move in the y direction with velocity $v_{\mathrm{F}} = d\varepsilon_{\mathrm{e/h}}/dk_y = -t\cos k_y$, as illustrated (for electrons) in Fig. 1. For small k_y the condition $\alpha > 0$ is satisfied for $|k_z| < k_0$, i.e., for k_z between the two Weyl points.

III. EQUILIBRIUM CURRENT

Superconductor–normal-metal heterostructures with a magnetic N region are known to exhibit an equilibrium current in the direction of $\boldsymbol{E}\times\boldsymbol{B}$, where here the role of the time-reversal breaking (magnetic) field $\boldsymbol{B}$ is played by the exchange field [described by the term proportional to β in $\mathcal{H}^{(\mathrm{W})}$ and here pointing in the z direction] and the role of the inversion-symmetry breaking (electric) field $\boldsymbol{E}$ is played by a confinement-potential gradient of the interface (here in the x direction) [57]. In our geometry we thus expect to find an equilibrium current in the y direction.

A. Scattering formulation

We calculate the equilibrium current density I_y as the derivative of the ground-state energy E to the vector potential A_y. The vector potential A_y enters the Bogoliubov–de Gennes Hamiltonian $\mathcal{H}$ of Eq. (16) via the standard substitution $k_y \to k_y - \nu_3 eA_y$. Then the equilibrium current I_y is

$$\begin{aligned} I_y &= \frac{1}{2}\sum_\tau \int_{-\infty}^{0} d\varepsilon\, \varepsilon \frac{\partial}{\partial A_y}\frac{dN_\tau(\varepsilon)}{d\varepsilon} \\ &= -\frac{1}{2}\sum_\tau \int_{-\infty}^{0} d\varepsilon \frac{\partial N_\tau(\varepsilon)}{\partial A_y}, \end{aligned} \tag{29}$$

where $dN_\tau(\varepsilon)/d\varepsilon$ is the density of states of the Hamiltonian $\mathcal{H}_\tau$ of Eq. (21) and $N_\tau(\varepsilon)$ is the cumulative density of states.

The density of states $dN_\tau(\varepsilon)/d\varepsilon$ is a sum of delta-function contributions for $|\varepsilon| < \Delta$ and continuous otherwise. In principle, $dN_\tau(\varepsilon)/d\varepsilon$ may depend on A_y in both the discrete and continuous parts of the spectrum [61]. To capture both contributions, we adopt a procedure used by Beenakker and one of us for the calculation of the Josephson effect in a chaotic quantum dot [62]. Following Ref. [62], we determine $N_\tau(\varepsilon)$ by matching solutions of the Bogoliubov–de Gennes equation $\mathcal{H}_\tau\psi = \varepsilon\psi$ in the superconducting region $x < 0$ and in the normal region $x > 0$. To this end, we insert an "ideal lead" between the superconducting region at $x < 0$ and the normal region at $x > 0$, described by the Hamiltonian of Eq. (21) with $\mathcal{M}_\tau = 0$. At the end of the calculation, the length of the ideal lead is sent to zero. In the ideal lead, the Bogoliubov–de Gennes equation is solved by the scattering states

$$\psi_{\tau;\nu,\pm}(x) = e^{\pm i\varepsilon x/t}|\nu, \pm\nu\tau\rangle, \tag{30}$$

where $|\nu,\sigma\rangle$ with $\nu,\sigma = \pm 1$ is an eigenspinor of ν_3 at eigenvalue ν and of σ_1 at eigenvalue σ. The eigenstates $\psi_{\tau;\nu,+}$ and $\psi_{\tau;\nu,-}$ represent solutions moving in the positive and negative x directions, respectively. The solutions with $\nu = 1$ are electron-like; the eigenstates with $\nu = -1$ are hole-like.

In the ideal-lead segment around $x = 0$, the full solution of the Bogoliubiov–de Gennes equation is a linear combination of the scattering states given in Eq. (30),

$$\psi_\tau(x) = \sum_\nu [a_{\tau,\nu}\psi_{\tau;\nu,+}(x) + b_{\tau,\nu}\psi_{\tau;\nu,-}(x)]. \tag{31}$$

Viewing the coefficients $a_{\tau,\nu}$ and $b_{\tau,\nu}$ as amplitudes of quasiparticles incident on and reflected from the normal region, respectively, we may relate them via the scattering matrix $S_\tau(\varepsilon)$ of the normal region

$$\begin{pmatrix}b_{\tau,+}\\ b_{\tau,-}\end{pmatrix} = S_\tau(\varepsilon)\begin{pmatrix}a_{\tau,+}\\ a_{\tau,-}\end{pmatrix}. \tag{32}$$

[The dependence of $S_\tau(\varepsilon)$ on k_y and k_z is kept implicit.] When seen from the superconductor, the coefficients a_ν represent the reflected amplitudes, whereas the coefficients b_ν represent the incident amplitude, so that one has the relation

$$\begin{pmatrix}a_{\tau,+}\\ a_{\tau,-}\end{pmatrix} = S_\tau^{(\mathrm{S})}(\varepsilon)\begin{pmatrix}b_{\tau,+}\\ b_{\tau,-}\end{pmatrix}, \tag{33}$$

where $S_\tau^{(\mathrm{S})}(\varepsilon)$ is the scattering matrix of the superconducting region. Upon combining Eqs. (32) and (33), one finds that nontrivial solutions of the Bogoliubov–de Gennes equation exist only if

$$\det\left[1 - S_\tau(\varepsilon)S_\tau^{(\mathrm{S})}(\varepsilon)\right] = 0. \tag{34}$$

Since $S_\tau(\varepsilon)$ and $S_\tau^{(\mathrm{S})}(\varepsilon)$ are analytic functions of ε in the upper half of the complex plane, we may directly obtain the cumulative density of states $N_\tau(\varepsilon)$ as [62]

$$\begin{aligned} N_\tau(\varepsilon) = -\frac{1}{\pi}\int \frac{dk_y dk_z}{(2\pi)^2}\mathrm{Im}\Big\{ &\ln\det\left[1 - S_\tau(\varepsilon^+)S_\tau^{(\mathrm{S})}(\varepsilon^+)\right] \\ &- \frac{1}{2}\ln\{\det[S_\tau(\varepsilon)]\} - \frac{1}{2}\ln\left\{\det\left[S_\tau^{(\mathrm{S})}(\varepsilon)\right]\right\}\Big\}, \end{aligned} \tag{35}$$

where $\varepsilon^+ = \varepsilon + i\eta$, η being a positive infinitesimal.

The second and third terms between the brackets in Eq. (35) do not contribute to the current after integration to k_y. The first term in Eq. (35) is analytic in the upper half of the complex plane and vanishes for $\mathrm{Im}\,\varepsilon \to \infty$. Shifting

the integration along the negative real axis to the positive imaginary axis, we then find

$$I_y = \int \frac{dk_z}{2\pi} \mathcal{I}_y(k_z), \tag{36}$$

where

$$\mathcal{I}_y(k_z) = -\frac{1}{2\pi} \sum_\tau \int \frac{dk_y}{2\pi} \mathrm{Re} \int_0^\infty d\omega \times \frac{\partial}{\partial A_y} \ln \det \left[1 - S_\tau(i\omega) S_\tau^{(\mathrm{S})}(i\omega)\right]. \tag{37}$$

Under particle-hole conjugation, the basis state $\psi_{\tau;\nu,\pm}(x)$ of Eq. (30) is mapped to $\mp\psi_{-\tau;-\nu,\pm}(x)$, while simultaneously inverting $\varepsilon \to -\varepsilon$ and $k_{y,z} \to -k_{y,z}$, and vice versa. For this choice of the scattering states, particle-hole symmetry imposes the condition

$$S_\tau(\varepsilon; k_y, k_z) = -\nu_1 S_{-\tau}^*(-\varepsilon; -k_y, -k_z)\nu_1. \tag{38}$$

Calculating the scattering matrix $S^{(\mathrm{S})}$ of the superconductor one obtains

$$S_\tau^{(\mathrm{S})}(\varepsilon) = e^{-i\gamma(\varepsilon)}\nu_1, \quad \gamma = \arccos(\varepsilon/\Delta), \tag{39}$$

which is the standard result for Andreev reflection off an s-wave spin-singlet superconductor [63]. The scattering matrix $S_\tau(\varepsilon)$ of the normal region is diagonal with respect to the particle-hole index ν,

$$S_\tau(\varepsilon; k_y, k_z) = \begin{pmatrix} r_\tau(\varepsilon; k_y, k_z) & 0 \\ 0 & -r_{-\tau}(-\varepsilon; -k_y, -k_z)^* \end{pmatrix}, \tag{40}$$

where $r_\tau(\varepsilon; k_y, k_z)$ is the reflection amplitude for electron-like quasiparticles. Inserting Eqs. (39) and (40) into Eq. (37) and performing a partial integration to k_y, we find

$$\mathcal{I}_y(k_z) = \frac{2e}{\pi} \int \frac{dk_y}{2\pi} \mathrm{Re} \int_0^\infty d\omega \frac{\partial r_+(i\omega; k_y, k_z)}{\partial k_y} \times \frac{r_-(i\omega; -k_y, -k_z)^*}{e^{2i\gamma(i\omega)} + r_+(i\omega; k_y, k_z) r_-(i\omega; -k_y, -k_z)^*}. \tag{41}$$

Because of the mirror antisymmetry at $\mu = 0$ given in Eq. (4), the reflection amplitudes satisfy $r_\tau(\varepsilon; k_y, k_z) = r_\tau(\varepsilon; -k_y, k_z)^*$, from which it follows that the current vanishes at $\mu = 0$. We use this feature of our model to focus our calculation on the derivative $d\mathcal{I}_y(k_z)/d\mu$ at small μ.

B. Reflection amplitudes of normal region

We calculate the reflection amplitude r_τ by expressing it in terms of the reflection and transmission amplitudes $r_\tau^{(\mathrm{W})}$, $r_\tau'^{(\mathrm{W})}$, $t_\tau^{(\mathrm{W})}$, and $t_\tau'^{(\mathrm{W})}$ of the normal region $0 < x < W$ and the reflection phase $i\tau$ of the insulator at $x > W$,

$$r_\tau = r_\tau^{(\mathrm{W})} + \frac{i\tau t_\tau'^{(\mathrm{W})} t_\tau^{(\mathrm{W})}}{1 - i\tau r_\tau'^{(\mathrm{W})}}. \tag{42}$$

In this notation, the unprimed amplitudes $r_\tau^{(\mathrm{W})}$ and $t_\tau^{(\mathrm{W})}$ refer to reflection and transmission from the normal region for particles incident at the interface with the superconductor (S), whereas the primed amplitudes $r_\tau'^{(\mathrm{W})}$ and $t_\tau'^{(\mathrm{W})}$ are for particles incident at the interface with the trivial insulator (I). Solving the scattering problem with the Hamiltonian of Eq. (21), we find the explicit expressions

$$r_\tau^{(\mathrm{W})}(\varepsilon; k_y, k_z) = r_\tau'^{(\mathrm{W})}(\varepsilon; -k_y, -k_z) = i\tau \frac{m(k_y, k_z) + \beta\tau - it\tau \sin k_y}{t\kappa_\tau \coth(\kappa_\tau W) - i(\varepsilon + \mu)}, \tag{43}$$

$$t_\tau^{(\mathrm{W})}(\varepsilon; k_y, k_z) = t_\tau'^{(\mathrm{W})}(\varepsilon; -k_y, -k_z) = \frac{t\kappa_\tau / \sinh(\kappa_\tau W)}{t\kappa_\tau \coth(\kappa_\tau W) - i(\varepsilon + \mu)}, \tag{44}$$

where we abbreviated

$$\kappa_\tau^2 t^2 = d_\tau(k_x, k_y)^2 - (\varepsilon + \mu)^2, \tag{45}$$

with

$$d_\tau(k_y, k_z) = \sqrt{t^2 \sin^2 k_y + [\beta + \tau m(k_y, k_z)]^2} \tag{46}$$

the gap in the k_z-dependent spectrum of the Hamiltonian shown in Eq. (21), see Eq. (5). The symmetry relation between the primed and unprimed reflection and transmission amplitudes is a consequence of the inversion symmetry from Eq. (15).

To evaluate the k_z-resolved current density $\mathcal{I}_y(k_z)$, it is convenient to consider the three-dimensional Hamiltonian $\mathcal{H}(k_x, k_y, k_z)$ as a family of two-dimensional Hamiltonians $\mathcal{H}(k_x, k_y)$ that parametrically depend on k_z. The two-dimensional Hamiltonian $\mathcal{H}^{(\mathrm{W})}(k_x, k_y)$ describes a trivial (two-dimensional) insulator if $\beta < m_0$ or if $m_0 < \beta < m_0 + 2t_z'$ and $|k_z| > k_0$, see Eqs. (6) to (8). It describes a (two-dimensional) topologically nontrivial Chern insulator if $m_0 < \beta < m_0 + 2t_z'$ and $|k_z| < k_0$ or if $\beta > m_0 + 2t_z'$.

For the calculation of the equilibrium current I_y, we find it convenient to parametrize the reflection amplitudes $r_\tau^{(\mathrm{W})}$, and $r_\tau'^{(\mathrm{W})}$ in terms of the transmission coefficient $T_\tau = |t_\tau^{(\mathrm{W})}|^2$ and the phase shifts ϕ_τ and ϕ_τ',

$$r_\tau^{(\mathrm{W})} = i\tau\sqrt{1 - T_\tau} e^{i\phi_\tau}, \quad r_\tau'^{(\mathrm{W})} = i\tau\sqrt{1 - T_\tau} e^{i\phi_\tau'}. \tag{47}$$

Expressions for the reflection phases ϕ_τ and ϕ_τ' can be obtained from Eq. (43). For small k_y, ε, and μ, the reflection phase ϕ_+ of the high-energy band is well approximated by

$$\phi_+(k_y, k_z) = \phi_+'(-k_y, -k_z) \approx (\varepsilon + \mu - k_y t)/d_+. \tag{48}$$

The approximations for the reflection phase for the low-energy band for small k_y, ε, and μ are different for the trivial regime $\beta < m_0$ or $|k_z| > k_0$ and the topological regime $\beta > m_0 + 2t_z'$ or $|k_z| < k_0$,

$$\phi_-(k_y, k_z) = \phi_-'(-k_y, -k_z) \approx \begin{cases} (\varepsilon + \mu + k_y t)/d_- & \text{trivial,} \\ \pi + (\varepsilon + \mu - k_y t)/d_- & \text{topological.} \end{cases} \tag{49}$$

The fact that $\phi_- = \pi$ at $k_y = 0$ in the topological case is what causes the appearance of the Fermi-arc surface states near $k_y = 0$. With the parametrization defined in Eqs. (47),

the reflection amplitude $r_\tau(\varepsilon; k_y, k_z)$ reads

$$r_\tau = i\tau e^{i\phi_\tau} \frac{e^{i\phi'_\tau} + \sqrt{1-T_\tau}}{e^{i\phi'_\tau}\sqrt{1-T_\tau}+1}. \tag{50}$$

C. k_z-resolved current density for large W

We will now discuss the k_z-resolved current $\mathcal{I}_y(k_z)$ well inside the trivial and topological regimes, so that the two-dimensional Hamiltonian $\mathcal{H}^{(\mathrm{W})}(k_x, k_y)$ describes a gapped phase with a gap magnitude on the order of the band width. The case that k_z is in the vicinity of k_0 will be addressed in Sec. III E.

For our calculation of $\mathcal{I}_y(k_z)$ we assume that the width W of the normal region is much larger than the lattice spacing (which is set to one). The energy scale corresponding to the inverse width, t/W, the pair potential Δ, and the chemical potential μ are considered to be much smaller that the band width $t \sim t' \sim t'_z$. The energy difference of the high- and low-energy bands $2m_0$ is considered to be on the order of the band width.

With this hierarchy of energy and length scales, the energy dependence of the reflection amplitudes of the normal region may typically be neglected when compared to the energy dependence of the phase shift γ for Andreev reflection from the superconductor. Also, one has $\kappa_\tau W \gg 1$, so that transmission is exponentially suppressed, $T_\tau \downarrow 0$. Assuming continuity of the current with $T_\tau \downarrow 0$, which we discuss in more detail in Appendix B, we may set

$$r_\tau(i\omega; k_y, k_z) = i\tau e^{i\phi_\tau(k_y,k_z)}, \tag{51}$$

where the reflection phase $\phi_\tau(k_y, k_z)$ of the normal region is evaluated at $\varepsilon = 0$ since the energy dependence is dominated by the energy dependence of the reflection phase $e^{-i\gamma}$ of the superconductor. This approximation breaks down if $e^{i\phi'_\tau} = -1$ because then the denominator in Eq. (50) vanishes for $T_\tau \downarrow 0$ so that the energy dependence of $r_\tau(\varepsilon; k_y, k_z)$ becomes important, which occurs if a Fermi-arc state at the surface at $x = W$ crosses the Fermi level. This case will be discussed in Sec. III D. With the approximation from Eq. (51), the ω-integration in Eq. (41) may then be performed, with the result

$$\mathcal{I}_y(k_z) = -\frac{e\Delta}{2}\int \frac{dk_y}{2\pi}\frac{\partial\phi_+}{\partial k_y} s(\phi)\sin(\phi/2), \tag{52}$$

where

$$\phi(k_y, k_z) = \phi_+(k_y, k_z) - \phi_-(-k_y, -k_z) \tag{53}$$

and $s(\phi) = \mathrm{sgn}\cos(\phi/2)$.

Effectively, the approximations used to derive Eq. (52) from the general result of Eq. (41) amount to restricting to contributions from the discrete part of the Andreev spectrum. (This approximation is known as the "short-junction limit" in the context of the Josephson effect.) To show that Eq. (52) represents the contribution from the discrete part of the Andreev spectrum, we note that, if we neglect the energy dependence of the reflection amplitudes from the normal region, Andreev bound states appear at discrete energies $\varepsilon_\pm(k_y, k_z)$ satisfying the quantization condition

$$e^{-i2\gamma(\varepsilon_\pm)} e^{i\phi_+(k_y,k_z)} e^{i\phi_-(-k_y,-k_z)} = 1. \tag{54}$$

Solving for $\varepsilon_\pm(k_y, k_z)$, one finds

$$\varepsilon_\pm(k_y, k_z) = \pm\Delta\cos(\phi/2). \tag{55}$$

The current associated with a single Andreev level is $\partial\varepsilon_\pm(k_y, k_z)/\partial A_y$. To find the total current we integrate over the contributions from all Andreev levels with energy $\varepsilon_\pm(k_y, k_z) < 0$,

$$\mathcal{I}_y(k_z) = \frac{1}{2}\sum_\pm \int \frac{dk_y}{2\pi}\frac{\partial\varepsilon_\pm}{\partial A_y}\Theta(-\varepsilon_\pm), \tag{56}$$

where the Heaviside function $\Theta(x) = 1$ if $x > 0$ and 0 otherwise. Upon substitution of Eq. (55) for $\varepsilon_\pm$, one recovers Eq. (52).

To find the derivative $d\mathcal{I}_y(k_z)/d\mu$ [recall that $\mathcal{I}_y(k_z) = 0$ for $\mu = 0$, see the discussion at the end of Sec. III A] we observe that from Eq. (43) we have

$$\frac{\partial\phi_\tau}{\partial\mu} = \frac{1}{d_\tau}, \tag{57}$$

where the gap $d_\tau(k_y, k_z)$ was defined in Eq. (46). For the μ-derivative of the k_z-resolved current $\mathcal{I}_y(k_z)$ we then find a "regular" contribution and a "singular" contribution, which follows from the derivative of the discontinuity of the step function $s(\phi)$ at $\phi = \pi \pmod{2\pi}$,

$$\frac{d\mathcal{I}_y(k_z)}{d\mu} = \frac{d\mathcal{I}_y(k_z)^{(\mathrm{r})}}{d\mu} + \frac{d\mathcal{I}_y(k_z)^{(\mathrm{s})}}{d\mu}, \tag{58}$$

with

$$\frac{d\mathcal{I}_y(k_z)^{(\mathrm{r})}}{d\mu} = -\frac{e\Delta}{4}\int\frac{dk_y}{2\pi}\left[\left(\frac{1}{d_+}-\frac{1}{d_-}\right)\frac{\partial\phi_+}{\partial k_y}\cos\frac{\phi}{2} - \frac{2}{d_+^2}\frac{\partial d_+}{\partial k_y}\sin\frac{\phi}{2}\right]s(\phi), \tag{59}$$

$$\frac{d\mathcal{I}_y(k_z)^{(\mathrm{s})}}{d\mu} = e\Delta\int\frac{dk_y}{2\pi}\frac{\partial\phi_+}{\partial k_y}\left(\frac{1}{d_+}-\frac{1}{d_-}\right)\delta(\phi-\pi), \tag{60}$$

where the delta function should be periodically extended with period 2π. In the limit of a large exchange field β, d_- is much smaller than d_+, and one may further approximate $d\mathcal{I}_y(k_z)/d\mu$ by restricting to the terms inversely proportional to d_-.

On the basis of Eqs. (59) and (60) we can compare $d\mathcal{I}_y(k_z)/d\mu$ in the trivial and topological regimes. The phases ϕ_+ and ϕ_- are shown versus k_y for typical model parameters in Figs. 2(a) and 2(b). In the topologically trivial case, generically both ϕ_+ and ϕ_- have a weak k_y-dependence and ϕ remains close to zero. In this case, the singular contribution $[d\mathcal{I}_y(k_z)/d\mu]^{(\mathrm{s})}$ is absent. Considering the "regular" contribution (59), we see that the dominant contribution to the total equilibrium current I_y comes from regions in which the gap d_- is smallest, which is in the vicinity of the Weyl points, i.e., for $|k_z| \downarrow k_0$. The sign of the equilibrium current is determined by the derivative $d\phi_+/dk_y$ near $k_y = 0$.

In the topological case, as a result of the band inversion from the sign change of $\beta - m(k_y, k_z)$, the phase ϕ_- decreases by 2π upon going from $k_y = -\pi$ to $k_y = \pi$. Hence, the singularity in the integrand at $\phi = \pi \pmod{2\pi}$ cannot be avoided. This gives rise to the singular contribution $[d\mathcal{I}_y(k_z)/d\mu]^{(\mathrm{s})}$ of Eq. (60). Since ϕ_- is close to π in the vicinity of $k_y = 0$, the

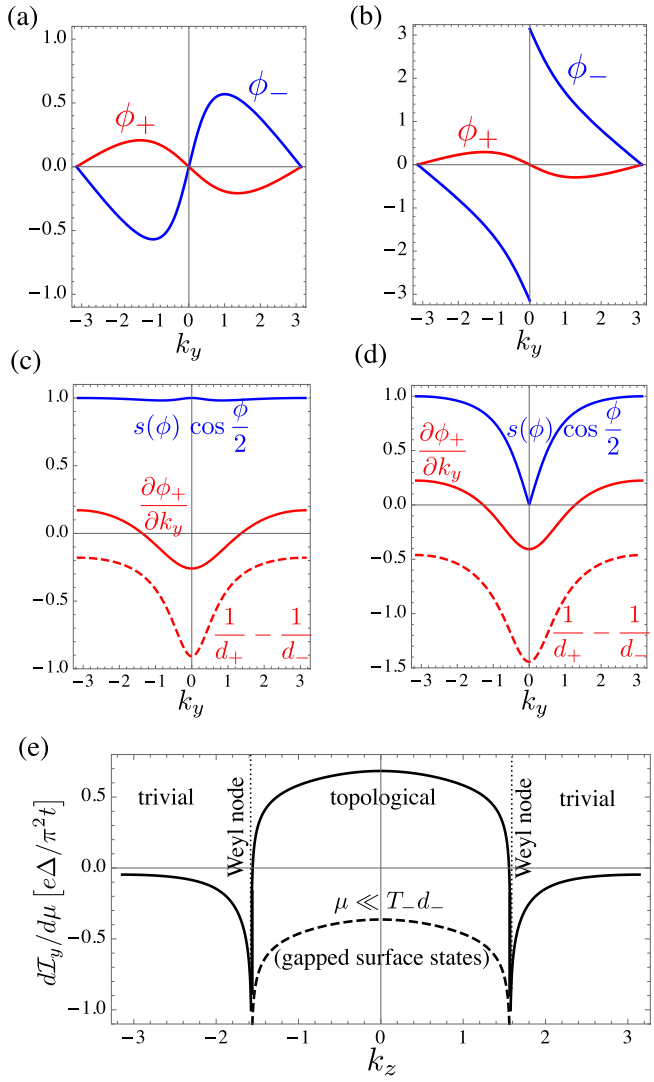

FIG. 2. (a,b) Reflection phases $\phi_\pm(k_y, k_z)$ at chemical potential $\mu \to 0$ and energy $\varepsilon = 0$ (after first taking the limit $W \to \infty$) for parameter choices corresponding to the (a) trivial and (b) topological regimes. (c,d) Factors $s(\phi)\sin(\phi/2)$ (blue), $(t/d_+ - t/d_-)$ (red, dashed), and $\partial\phi_+/\partial k_y$ (red, solid) for the same parameter choices as in (a) and (b), respectively. (e) k_z-resolved equilibrium current $\mathcal{I}_y(k_z)$ as a function of k_z from Eq. (58) (solid curve). The sign of the current changes if k_z goes from the topological region (k_z between the Weyl nodes at $\pm k_0$) to the trivial region. The dashed line shows the result at ultrasmall chemical potential within the finite-size gap of surface states, see Eq. (65). The parameters are $m_0 = 0.5\,t$, $\beta = 1.5\,t$, $t = t' = t'_z = 1$. In panels (a) and (c) we further set $k_z = 1$; in panels (b) and (d) we set $k_z = 2.6$.

integrand in Eq. (60) has support precisely where the derivative $\partial\phi_+/\partial k_y$ is maximal, see Fig. 2(c). As a consequence, in the topological regime, the total current $d\mathcal{I}_y(k_z)/d\mu$ has larger magnitude and opposite sign when compared to the trivial regime, see Fig. 2(e).

To obtain an explicit expression for a special parameter choice well inside the topological regime, one may consider $k_z = 0$ and $\beta = m_0 + t'$, $t' = t$, in which case $\kappa_- = 1$ and $\phi_-(k_y, 0) \approx \pi - k_y$ for all k_y. Additionally assuming a large gap $d_+ \approx \beta + m_0 \gg t$, so that $\phi_+(k_y, 0) \approx -[t/(m_0 + \beta)]\sin k_y$, the current becomes

$$\frac{d\mathcal{I}_y(0)}{d\mu} \approx \frac{2e\Delta}{3\pi(\beta + m_0)}. \tag{61}$$

For the trivial case we consider the leading-order term in β/t, since the current vanishes at $\beta = 0$, and take $m_0 = t = t'$ and $k_z = 0$, which gives

$$\frac{d\mathcal{I}_y(0)}{d\mu} \approx -\frac{e\Delta\beta}{12\pi t^2}. \tag{62}$$

Comparing Eqs. (61) and (62) also shows the opposite signs of the equilibrium current in the two regimes.

D. Finite-size effects

For small transmission coefficient T_- of the low-energy band, the presence of the Fermi-arc states at the interface with the trivial insulator at $x = W$ causes a narrow resonance in the reflection amplitude $r_-(\varepsilon; k_y, k_z)$. This resonance occurs, when the denominator in Eq. (50) is approximately zero, $e^{i\phi'_\tau} \approx -1$. In this case, the assumption that the energy dependence of $r_-(\varepsilon; k_y, k_z)$ can be neglected when compared to the energy dependence of the Andreev reflection phase $e^{-i\gamma(\varepsilon)}$ is obviously violated, despite the fact that the gap $d_- \gg \Delta$.

For the minimal model we consider in this article, this issue affects the topological regime $\beta > m_0$, $|k_z| < k_0$ only. Here we consider the case of small $\mu \ll t$, so that the resonance appears in the vicinity of $k_y = 0$. For small transmission coefficient T_-, the full reflection amplitude r_- of Eq. (50) may then be well approximated as

$$r_- = -ie^{i\phi_-} w(k_y t + \varepsilon + \mu), \tag{63}$$

with

$$w(\varepsilon) = \frac{2\varepsilon - iT_- d_-}{2\varepsilon + iT_- d_-}. \tag{64}$$

Since $w(k_y t + i\omega + \mu) \approx 1$ if $|k_y t + i\omega + \mu| \gtrsim T_- d_-$, the presence of the factor $w(k_y t + i\omega + \mu)$ has little effect on the integrand in Eq. (41) in the limit of small transmission T_- if $\mu \gg T_- d_-$, except for a small integration region around $k_y t \approx -\mu$ and $\omega \lesssim T_- d_-$. Because of the smallness of the integration region in which w significantly differs from unity, the net finite-size effect on $d\mathcal{I}_y(k_z)/d\mu$ after integration over k_y and ω is small and goes to zero if $T_- \to 0$. For $\mu \lesssim T_- d_-$ this conclusion cannot be drawn, however, because the singularity in the fraction in Eq. (64) coincides with the singularity of the integrand in $d\mathcal{I}_y(k_z)/d\mu$, which led to the singular contribution shown in Eq. (60).

To analyze this limit of "ultrasmall" chemical potential μ in further detail, we observe that the singular contributions of the integration in Eq. (41) from the vanishing of the denominator and from the finite-size factor $w(k_y t + i\omega + \mu)$ are limited to a small interval $-\delta < k_y < \delta$ around $k_y = 0$, where $\delta \ll 1$ may be chosen large enough that $w(\pm\delta t + \mu + i\omega) \approx 1$. It follows that the "regular" contribution of Eq. (59) to $d\mathcal{I}_y(k_z)/d\mu$, which is associated with momenta k_y outside this interval, is unaffected by the finite-size effects. On the other hand, as we show in detail in Appendix A, upon inclusion of the finite-size effects the integrand of the singular contribution $d\mathcal{I}_y(k_z)^{(s)}/d\mu$ is multiplied by a negative factor

$-(d_+ + d_-)/(d_+ - d_-)$, when compared to the result given in Eq. (60) for $\mu \gg T_- d_-$. Hence for ultrasmall chemical potential $\mu \ll T_- d_-$ we find

$$\frac{d\mathcal{I}_y(k_z)}{d\mu} = \frac{d\mathcal{I}_y(k_z)^{(\mathrm{r})}}{d\mu} + \frac{d\mathcal{I}_y(k_z)^{(\mathrm{s})}}{d\mu}, \tag{65}$$

with $[d\mathcal{I}_y(k_z)/d\mu]^{(\mathrm{r})}$ given by Eq. (59) and

$$\frac{d\mathcal{I}_y(k_z)^{(\mathrm{s})}}{d\mu} = e\Delta \int \frac{dk_y}{2\pi} \frac{\partial \phi_+}{\partial k_y} \left(\frac{1}{d_+} + \frac{1}{d_-} \right) \delta(\phi - \pi). \tag{66}$$

The sign change of the singular contribution leads to a significant *reduction* of the equilibrium current in the case of an ultrasmall chemical potential $\mu \ll T_- d_-$, when compared to the case $\mu \gg T_- d_-$.

To obtain an order-of-magnitude estimate, we again set $k_z = 0$ and consider the well-established topological regime $\beta = m_0 + t'$, $t' = t$, $k_z = 0$, $\beta + m_0 \gg 1$, for which we find that

$$\frac{d\mathcal{I}_y(0)}{d\mu} \approx -\frac{e\Delta}{3\pi(\beta + m_0)} \tag{67}$$

if $\mu \ll T_- d_-$. A comparison to Eq. (61) shows that at ultrasmall chemical potential the equilibrium current is approximately $-1/2$ times the current at finite μ.

Physically, the energy $\sim T_- d_- \sim t\, e^{-2W}$ that separates the regimes of "ultrasmall" and "finite" μ is associated with the finite-size gap of the Fermi-arc surface states, whose wavefunctions decay exponentially away from the surfaces. Based on our result that in the topological regime the equilibrium current is strongly modified when the chemical potential is inside this finite-size gap, we interpret the difference between the finite-μ and ultrasmall-μ limits as the contribution of the topological surface states to $d\mathcal{I}_y/d\mu$. The difference between the large-μ and small-μ limits involves the singular contribution $[d\mathcal{I}_y/d\mu]^{(\mathrm{s})}$ only. In the well-established topological regime the surface-state contribution assumes the value $2[d\mathcal{I}_y/d\mu]^{(\mathrm{s})}$, with $[d\mathcal{I}_y/d\mu]^{(\mathrm{s})}$ given in Eq. (60).

E. Total current density

The full equilibrium current density I_y involves the integral of $\mathcal{I}_y(k_z)$ over k_z. The k_z-resolved current density $\mathcal{I}_y(k_z)$ is calculated in Sec. III C, for the case that the normal region is gapped at momentum k_z and that the gap $d_\tau \gg \Delta$. This condition is no longer satisfied for the low-energy band if k_z is in the immediate vicinity of the Weyl points because $d_- \to 0$ there.

That the results of Sec. III C cease to be valid if d_- becomes small in comparison to Δ is also reflected in the expression in Eq. (58) for $d\mathcal{I}_y(k_z)/d\mu$, which diverges $\propto \Delta/d_-$ if $d_-/\Delta \to 0$. This divergence should be cutoff for $d_- \sim \Delta$. To see this, we evaluate $d\mathcal{I}_y(k_z)/d\mu$ in the opposite limit $d_- \ll \Delta$, in which we may neglect the energy dependence of the Andreev reflection phase $e^{-i\gamma(\varepsilon)}$ and of the reflection amplitude r_+ of the high-energy band, but keep the full energy dependence of the reflection amplitude r_- of the low-energy band.

Starting point of our calculation is Eq. (41). Since r_- depends on energy ε and chemical potential μ through the combination $\varepsilon + \mu$ only, upon analytic continuation $\varepsilon \to i\omega$, one has $\partial r_-^*/\partial\mu = i\partial r_-^*/\partial\omega$. When calculating $d\mathcal{I}_y(k_z)/d\mu$, the integrand in Eq. (41) then is a total derivative to ω and we find

$$\frac{d\mathcal{I}_y(k_z)}{d\mu} = \frac{2e}{\pi} \int \frac{dk_y}{2\pi} \mathrm{Re}\, \frac{\partial \phi_+}{\partial k_y} \frac{1}{e^{-i\phi} + 1}, \tag{68}$$

where, as before, $\phi(k_y, k_z) = \phi_+(k_y, k_z) - \phi_-(-k_y, -k_z)$. Using $\mathrm{Re}\, 1/(e^{-i\phi} + 1) = 1/2 - \pi\delta(\phi - \pi)$ we find that $d\mathcal{I}_y(k_z)/d\mu \sim e\partial\phi_+/\partial k_y$, which is the same order-of-magnitude estimate as one would obtain from Eq. (58) by cutting off the small-d_--divergence at $d_- \sim \Delta$. [We note that the condition $d_- \ll \Delta$ may not be fulfilled for all k_y simultaneously, so that, strictly speaking, the approximations leading to Eq. (68) do not apply to the full range of the k_y-integration. This, however, does not affect the order-of-magnitude estimate of $d\mathcal{I}_y(k_z)/d\mu \sim e\partial\phi_+/\partial k_y$ that follows from Eq. (68).]

We thus find that $d\mathcal{I}_y(k_z)/d\mu \sim e\partial\phi_+/\partial k_y$ is a regular function of k_z in the vicinity of the Weyl points at $k_z = \pm k_0$. Since the range of momenta k_z affected by the violation of the condition $d_\tau \gg \Delta$ is correspondingly small, we conclude that the contribution of the Weyl points to the total current $dI_y/d\mu$ is small and that one may obtain $dI_y/d\mu$ by integration of the k_z-resolved result of Eq. (58) for $d\mathcal{I}_y(k_z)/d\mu$, omitting the immediate vicinity of the Weyl points from the integration range.

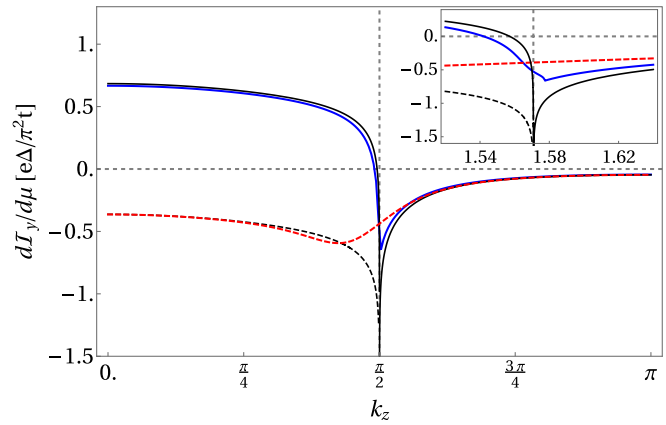

FIG. 3. k_z-resolved equilibrium current $d\mathcal{I}_y/d\mu$. The superconducting gap $\Delta = 0.01\,t$; the other parameters are the same as in Fig. 2. The solid blue and dashed red curves are obtained from Eq. (41) with finite chemical potential $\mu = 0.01\,t$ and $\mu = 10^{-6}\,t$, respectively. The width of the normal region is $W = 300$ and $W = 5$, respectively. The solid and dashed black curves are obtained from Eqs. (58) and (65), respectively. The inset shows a closeup at the Weyl node at $k_0 \approx \pi/2$. The discontinuity in the derivative of $d\mathcal{I}_y/d\mu$ vs k_z near k_0 is a finite-size effect and disappears upon further increasing W.

F. Numerical results

In Fig. 3 we compare the k_z-resolved equilibrium current $d\mathcal{I}_y(k_z)/d\mu$ obtained directly from Eq. (41) with the approximation of Eq. (58). We find excellent agreement away from the Weyl points. We observe that $d\mathcal{I}_y(k_z)/d\mu$ has opposite signs for $\mu \ll T_- d_-$ and $\mu \gg T_- d_-$ in the topological regime (k_z between the Weyl points), while there is no difference between the cases of large and small μ in the trivial regime. Except for the finite-size effect at ultrasmall chemical

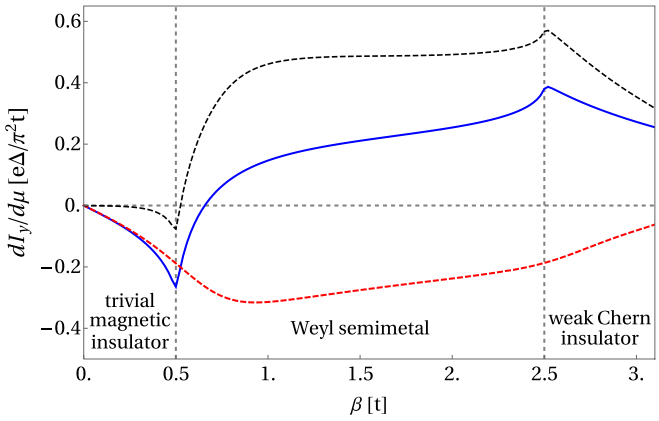

FIG. 4. Equilibrium current $dI_y/d\mu$ as a function of the exchange field β. The solid blue curve is for finite chemical potential $\mu = 0.01\,t$ and width $W = 300$, which meets the condition $\mu \gg T_- d_-$ for most of reciprocal space. The dashed red curve is for ultrasmall chemical potential $\mu = 10^{-6}\,t$ and width $W = 5$, which meets the condition $\mu \ll T_- d_-$ for most of reciprocal space. The black dashed curve shows the difference of these two cases, which is the contribution to $dI_y/d\mu$ associated with the Fermi arcs. Other parameters are same as in Figs. 2 and 3.

potentials, we observe only a weak dependence on the width W of the normal region, which is bound to the small vicinity ($d_- \lesssim \Delta$) of Weyl nodes (data not shown).

Figure 4 shows the total current density $dI_y/d\mu$, see Eq. (36), as a function of the exchange field β. For comparison, the ultrasmall-μ limit and the difference between the cases of ultrasmall and finite μ are also shown (dashed curves in Fig. 4). The current vanishes at $\beta = 0$ because the system is time-reversal invariant there. Its magnitude increases with β in the trivial insulator regime $\beta < m_0$. Upon entering the Weyl-semimetal regime, $dI_y/d\mu$ receives an upturn due to the positive contribution of the Fermi arcs. In the weak Chern insulator regime $\beta > m_0 + 2t_z'$, $dI_y/d\mu$ decreases upon (further) increasing β, but the difference between ultrasmall and finite chemical potential μ (dashed curve) persists.

To understand the apparent plateau in the Weyl-semimetal region $m_0 < \beta < m_0 + 2t_2'$ and the decrease with β in the Chern-insulator regime $\beta > m_0 + 2t_z'$, we note that the order of magnitude of the contribution of Fermi arcs (the difference between $dI_y/d\mu$ for $\mu \gg T_- d_-$ and $\mu \ll T_- d_-$) can be estimated from the difference of Eqs. (61) and (67), multiplying by the distance $2k_0$ between the Weyl points in the topological region,

$$\frac{dI_y^{\mathrm{FA}}}{d\mu} \sim \frac{e\Delta k_0}{\beta + m_0}, \tag{69}$$

where one needs to set $k_0 = \pi$ in the Chern-insulator regime. The apparent plateau in the Weyl-semimetal regime appears because the increase of the factor k_0 in the numerator with β is compensated by the increase of the denominator. In the Chern-insulator regime, the numerator in Eq. (69) is independent of β, whereas the denominator continues to increase with β, explaining the decrease of the current in the Chern-insulator regime. Note that k_0 has a singular dependence on β at the boundaries of the Weyl-semimetal regime at $\beta = m_0$ and $\beta = m_0 + 2t_z'$, see Eq. (7), which relates to the sharp upturns of the current. We verified that these sharp features are eliminated if $dI_y/d\mu$ is considered as a function of the node separation $2k_0$ in the Weyl-semimetal regime (data not shown).

IV. DISCUSSION AND CONCLUSION

We investigated the equilibrium current in a minimal model describing an *SN* heterostructure, where *S* is a conventional *s*-wave superconductor and, depending on the value of the exchange field β, the normal region (*N*) can be a magnetic insulator with a topologically trivial band structure, a Weyl semimetal with broken time-reversal symmetry, or a three-dimensional weak Chern insulator. The constituents of the heterostructure are microscopically inversion-symmetric, so that inversion symmetry is broken only by the heterostructure geometry. In all three regimes, time-reversal symmetry is broken by the exchange field.

In the trivial-insulator regime we find an equilibrium current that is proportional to the exchange field β at small β. It quantifies the interface current of a superconductor–magnetic insulator heterostructure, which is known to be generally possible in the presence of spin-orbit coupling. Previously such an equilibrium current has been predicted only for a system with interfacial Rashba spin-orbit coupling [57], instead of the intrinsic spin-orbit coupling considered here.

In the topological regime of a Weyl semimetal or a weak Chern insulator the current shows a qualitatively different behavior. Upon entering the topological regimes the β-dependence of the equilibrium current abruptly changes, causing a reversal of the sign of the current well inside the topological regime. The decisive contribution comes from the topological surface states, which we can identify within a minimal model (motivated by materials of the Bi_2Se_3 family [10]) by comparing the equilibrium currents for a chemical potential inside and above the finite-size gap of the surface states. In contrast, the Weyl nodes of the bulk band structure, which the Fermi arcs connect, do not give a significant contribution to the equilibrium current.

That we find a large contribution of Fermi arcs and an insignificant contribution of Weyl nodes relates to previous studies which found that the bulk states of an inversion-symmetric, magnetic Weyl semimetal are mainly unaffected by superconductivity due to a "chirality blockade" [22]. Accordingly, we expect that this would change if the chirality blockade is lifted, which happens when at least one of the constituents of the heterostructure breaks the microscopic inversion symmetry [22]. In our model, the chirality blockade manifests itself through the fact that Andreev reflection from the superconductor switches quasiparticles between the topologically trivial high-energy band and the (potentially) topologically nontrivial low-energy band. It is this connection of the trivial and the nontrivial band by the superconducting pairing that also makes the magnitude of the equilibrium current non-universal in both the topologically trivial and nontrivial parameter regimes.

Whereas the "chirality blockade" prevents the bulk Weyl points to be strongly affected by the proximity superconductivity, Fermi-arc surface states at the interface with the

superconductor, on the other hand, undergo a renormalization of their effective charge [58], which, however, is weak because of the chirality blockade. Relating the Fermi-arc current contribution of Eq. (69) to the charge renormalization of Fermi arcs one can interpret the former in terms of an uncompensated chiral current of surface states. Specifically, one can consider that each Fermi arc contributes to the current density

$$\frac{dI_y^{(\mathrm{arc})}}{d\mu} = \mathrm{sgn}\,(v)\frac{k_0 q}{(2\pi)^2}, \tag{70}$$

where v is the velocity of the Fermi arc and q the effective charge. The Fermi-arc contribution to the current of the Fermi arcs is reproduced if the charge at the superconductor interface is renormalized to

$$q \sim -e[1-\Delta/(\beta+m_0)], \tag{71}$$

while the charge of the opposite surface remains unaffected ($q=-e$). The sign of the Fermi-arc velocity is discussed in Sec. II and is illustrated in Fig. 1.

The contribution of Fermi arcs can be seen as a real-space counterpart to the superconductivity-enabled equilibrium chiral magnetic effect [11,12], in which a disbalance of chiral Landau levels of a pair of Weyl Fermions is produced by current- or flux-biased bulk superconductivity acting asymmetrically in momentum space on the chiral Landau levels. The fundamental connection of chiral Landau levels and Fermi arcs allows for the complementary effect that we just described. The differences between chiral Landau levels and Fermi arcs are that the Fermi arcs continue to exist in zero magnetic field and are separated in real space. Our work shows that these differences can be used to realize the equilibrium chiral magnetic effect via the superconducting proximity effect, without flux or current bias, and at zero magnetic field.

Relevant materials where the Fermi-arc contribution to the equilibrium current should be important are magnetic Weyl semimetals, such as GdPtBi [64] and $Co_3Sn_2S_2$ [53]. Our work, however, shows that the experimental identification of the Fermi-arc contribution is challenging because the equilibrium current is not exclusively due to Fermi arcs. The isolation of the Fermi-arc contribution that we could obtain in the minimal model (relying on an ultrasmall chemical potential or an ultrasmall, constant width of the Weyl semimetal, and mirror antisymmetry) does not seem to be experimentally realizable on the basis of existing materials. We believe, however, that characteristic signatures or other peculiar effects may be found in further studies of the equilibrium current, such as exploring its response to external magnetic fields.

ACKNOWLEDGMENTS

The authors would like to thank I. Adagideli and O. Kashuba for valuable discussions. This research was supported by the German Science Foundation (DFG) through Grant No. 18688556 and by project A02 of the CRC-TR 183 "Entangled States of Matter."

APPENDIX A: $[d\mathcal{I}_y(k_z)/d\mu]^{(\mathrm{s})}$ FOR $\mu \downarrow 0$

To show that the singular contribution to $d\mathcal{I}_y/d\mu$ changes sign in the limit $\mu \ll T_- d_-$ of an "ultrasmall" chemical potential (as compared to the case $\mu \gg T_- d_-$ of a "finite" chemical potential), we consider the regime of small k_y and μ in more detail. The equilibrium current for finite W is found from Eq. (41) by replacing $r_+ r_-^*$ by $-e^{i\phi}w^*$, where the function $w(\mu+i\omega-k_y t)$ is given in Eq. (64), and by restricting the k_y-integration to the interval $-\delta < k_y < \delta$,

$$\mathcal{I}_y(k_z)^{(\mathrm{s})} = \frac{2e}{\pi}\int_{-\delta}^{\delta}\frac{dk_y}{2\pi}\mathrm{Im}\int_0^\infty d\omega \frac{\partial\phi_+}{\partial k_y}\frac{w^*}{e^{2i\gamma(\omega)-i\phi}-w^*}. \tag{A1}$$

The integration boundaries $\pm\delta$ are chosen such that, on the one hand, $w\approx 1$ for $|k_y|=\delta$, whereas, on the other hand, $\delta \downarrow 0$ as $T_- \to 0$.

To find $[d\mathcal{I}_y(k_z)/d\mu]^{(\mathrm{s})}$, we have to differentiate the integrand in Eq. (A1) to μ. Using that for small k_y one has $\partial w/\partial\mu = -(1/t)\partial w/\partial k_y$ and $\partial\phi/\partial\mu = (1/d_+ - 1/d_-) = -(1/t)\partial\phi/\partial k_y - 2/d_-$ and using that ϕ_+ is an odd function of k_y for $\mu\to 0$, so that we may treat $\partial\phi_+/\partial k_y$ as a constant inside the integration range $-\delta < k_y < \delta$, we obtain

$$\frac{d\mathcal{I}_y(k_z)^{(\mathrm{s})}}{d\mu} = \frac{2e}{\pi}\int_{-\delta}^{\delta}\frac{dk_y}{2\pi}\mathrm{Im}\int_0^\infty d\omega\frac{\partial\phi_+}{\partial k_y} \times\left(-\frac{1}{t}\frac{d}{dk_y}-\frac{2}{d_-}\frac{\partial}{\partial\phi}\right)\frac{w^*}{e^{2i\gamma(\omega)-i\phi}-w^*}. \tag{A2}$$

Since the first term between the brackets, which is proportional to d/dk_y, is a total derivative and since $w^*\approx 1$ at both ends of the integration domain, we may set $w^*\to 1$ in the integrand when evaluating the first term. This allows us to relate the first term to the equilibrium current at finite μ. Again using that $(1/t)\partial\phi/\partial k_y = -(1/d_+ + 1/d_-) = (d_+ + d_-)/(d_+ - d_-)\partial\phi/\partial\mu$, we recognize that the first term is $-(d_+ + d_-)/(d_+ - d_-)$ times the singular contribution of Eq. (60).

The second term between the brackets vanishes to leading order in Δ/d_-: To leading order in Δ/d_- the energy dependence in w^* can be neglected and the ω integration can be performed similarly as when going from Eq. (41) to Eq. (52) with the phase modified by w^*, which approaches 1 upon taking the limit $T_-\to 0$. The whole integrand is thus nonsingular in this limit and, upon integration, the term vanishes for $T_-\to 0$ due to the vanishing integration range.

APPENDIX B: CONTINUITY OF THE CURRENT IN THE LIMIT $T_- \downarrow 0$

In the main text we derived the current at the transmission amplitude set to zero from the beginning. Here we repeat the calculation in a more careful way, taking the limit $T_-\to 0$ at the end, to show that the current is a continuous function of T_- at $T_- = 0$. For simplicity we only consider the well-established topological regimes at $k_z = 0$, $\beta = m_0 + t$, and $t = t' = t_z'$. The goal is thus to reproduce Eqs. (61) and (67).

Starting point is Eq. (41), where we set $k_z = 0$,

$$\mathcal{I}_y(0) = \frac{2e}{\pi}\int\frac{dk_y}{2\pi}\mathrm{Re}\int_0^\infty d\omega\frac{\partial r_+(i\omega;k_y,0)}{\partial k_y} \times\frac{r_-(i\omega;-k_y,0)^*}{e^{2i\gamma(i\omega)}+r_+(i\omega;k_y,0)r_-(i\omega;-k_y,0)^*}. \tag{B1}$$

We consider leading order in the gap $d_+ \approx \beta + m_0$ of the high-energy band, allowing to approximate $r_+^{(\mathrm{W})} = i\exp[-it\sin k_y/(\beta+m_0)]$ and leading to

$$\mathcal{I}_y(0) = \frac{2et}{\pi(\beta+m_0)}\int\frac{dk_y}{2\pi}\cos k_y\,\mathrm{Re}\int_0^\infty d\omega \times \frac{r_-(i\omega;-k_y,0)^*}{e^{2i\gamma(i\omega)}+ir_-(i\omega;-k_y,0)^*}. \tag{B2}$$

For the nontrivial band we take the full reflection amplitude of Eq. (50)

$$r_- = -ie^{i\phi_-}\frac{e^{i\phi'_-}+\sqrt{1-T}}{e^{i\phi'_-}\sqrt{1-T}+1}, \tag{B3}$$

where for brevity we have written T instead of T_-. In the well-established topological regime at $k_z = 0$, $\beta = m_0 + t$, and $t = t' = t'_z$, the reflection phase for the nontrivial band is $\phi_-(k_y,k_z) = \pi + \mu/t - k_y$. Further, we introduce $Z = \exp(-ik_y)$ and use $dk_y\cos k_y = idZ(1+Z^2)/2Z^2$, as well as $\omega = \Delta\sinh\zeta$ and $d\omega = d\zeta\,\Delta\cosh\zeta$ (so that $e^{2i\gamma} = -e^{2\zeta}$) to obtain

$$\mathcal{I}_y(0) = -\frac{\Delta\, e\, t}{\pi(\beta+m_0)\sqrt{1-T}}\mathrm{Re}\int_0^\infty d\zeta\oint\frac{dZ}{2\pi i}\cosh\zeta \times \frac{i(e^{-i\mu/t}-\sqrt{1-T}Z)(1+Z^2)}{Z(Z-Z_-)(Z-Z_+)}, \tag{B4}$$

where

$$Z_\pm = e^\zeta\frac{\pm i\sqrt{\sin^2(i\zeta-\mu/t)-T}+\cos(i\zeta-\mu/t)}{\sqrt{1-T}}. \tag{B5}$$

The integration contour of Z is the unit circle in the complex plane enclosing two poles, one at $Z=0$ and the other at $Z = Z_+$.

For $T = 0$ only the pole at $Z = 0$ contributes to the integral, due to cancellation of the $(Z - Z_+)$ term of the denominator with the first term of the numerator in Eq. (B4), and it gives

$$\mathcal{I}_y^{(0)}(0) = -\frac{\Delta\, e\, t}{\pi(\beta+m_0)}\mathrm{Im}\int_0^\infty d\zeta\cosh\zeta\; e^{-2\zeta-i\mu/t}, \tag{B6}$$

which for $\mu \ll t$ evaluates to

$$\frac{d\mathcal{I}_y^{(0)}(0)}{d\mu} = \frac{2e\Delta}{3\pi(\beta+m_0)}, \tag{B7}$$

reproducing Eq. (61).

For $T > 0$ both poles at $Z = 0$ and $Z = Z_+$ contribute to the integration. The contribution of the $Z = 0$ pole gives the same as the result Eq. (B6) for $T = 0$ up to a factor of $1/\sqrt{1-T} \to 1$.

The contribution to the integral from the pole at $Z = Z_+$ is

$$\mathcal{I}_y^{(1)}(0) = -\frac{e\Delta}{2\pi(\beta+m_0)}\mathrm{Im}\int_0^\infty d\zeta\, g(i\zeta-\mu/t) \times [z(i\zeta-\mu/t)(1+e^{2\zeta}) + z^{-1}(i\zeta-\mu/t)(1+e^{-2\zeta})], \tag{B8}$$

where we abbreviated

$$g(i\zeta-\mu/t) = \frac{e^{-i\mu/t}-\sqrt{1-T}Z_+}{\sqrt{1-T}(Z_+-Z_-)}, \tag{B9}$$

$$z(i\zeta-\mu/t) = e^{-\zeta}Z_+. \tag{B10}$$

(One verifies that g and z are functions of $i\zeta - \mu/t$ only.) Since it contributes for $T > 0$ only, the pole at Z_+ can be seen to represent a contribution to the equilibrium current from the Fermi arc at the insulating side of the semimetal. To estimate this contribution in the limit of small T, we note that the difference $Z_+ - Z_-$ is

$$Z_+ - Z_- = 2ie^\zeta\sqrt{\frac{\sin^2(i\zeta-\mu/t)-T}{1-T}}. \tag{B11}$$

To further evaluate this expression in the limit of small transmission T, we note that for $T \ll 1$ one has

$$Z_+ = e^{-i\mu/t}\Big[1 - i\frac{T}{2}\cot(i\zeta-\mu/t)+\cdots\Big]. \tag{B12}$$

In the limit of large ζ, this expansion is convergent and gives a numerator of order T in Eq. (B8). Hence, for large ζ, the integral in Eq. (B8) is convergent and of order T. If $\mu \neq 0$ this conclusion applies to the entire integration domain $\zeta > 0$, so that we conclude that the finite-T correction to the result shown in Eq. (B6) is of order T and smoothly vanishes for $T \downarrow 0$ if $\mu \neq 0$. The case $\mu = 0$ is different because then the expansion shown in Eq. (B12) is singular for $\zeta \to 0$. In the limit of small ζ one finds, if $\mu = 0$, that

$$g(i\zeta) = -\frac{\sqrt{\zeta^2+T}-\zeta}{2\sqrt{\zeta^2+T}} = -\frac{T}{2\sqrt{\zeta^2+T}(\sqrt{\zeta^2+T}+\zeta)}. \tag{B13}$$

We now divide up the ζ integral into a region $0 < \zeta < T^{\alpha/4}$ and a region $T^\alpha < \zeta$ with $0 < \alpha < 1/2$. In the former region, the remaining factors of the integration are approximately constant and integration of Eq. (B13) gives a contribution to $\mathcal{I}_y^{(1)}(0)$ that is of order $\sqrt{T}$. In the region $\zeta > T^\alpha$ one may still use the small-T expansion from Eq. (B12) to arrive at a systematic expansion around the result at $T = 0$. Since both contributions to the integral vanish in the limit $T \to 0$, we conclude that $\mathcal{I}_y^{(1)}(0) \to 0$ for $T \to 0$ even if $\mu = 0$, although the convergence may be slower than for generic μ.

We now consider the derivative of (B8) with respect to μ at $\mu = 0$ before taking the limit $T \to 0$. We use that $d/d\mu = (i/t)d/d\zeta$ acting on $z(i\zeta - \mu/t)$ and $g(i\zeta - \mu/t)$, to obtain

$$\frac{d\mathcal{I}_y^{(1)}(0)}{d\mu} = -\frac{e\Delta}{2\pi(\beta+m_0)d_-}\mathrm{Re}\int_0^\infty d\zeta(1+e^{2\zeta}) \times \frac{d}{d\zeta}g(i\zeta)z(i\zeta) + (1+e^{-2\zeta})\frac{d}{d\zeta}\frac{g(i\zeta)}{z(i\zeta)}. \tag{B14}$$

Using

$$\lim_{T\to0}\frac{g(0)}{z(0)} = \lim_{T\to0}g(0)z(0) = -\frac{1}{2}, \tag{B15}$$

partial integration gives

$$\frac{d\mathcal{I}_y^{(1)}(0)}{d\mu} = -\frac{e\Delta}{\pi(\beta+m_0)}\left[1 - \mathrm{Re}\int_0^\infty d\zeta\left(e^{2\zeta}g(i\zeta)z(i\zeta) - e^{-2\zeta}\frac{g(i\zeta)}{z(i\zeta)}\right)\right]. \tag{B16}$$

The remaining integral vanishes for $T \to 0$ similarly as the current in (B8) at $\mu = 0$ as shown above, hence

$$\frac{d\mathcal{I}_y^{(1)}(0)}{d\mu} = -\frac{e\Delta}{\pi(\beta+m_0)}. \tag{B17}$$

Thus for the total current $\mathcal{I}_y^{(0)}(0) + \mathcal{I}_y^{(1)}(0)$ in the ordered limit $\mu \to 0$, $T \to 0$ we obtain

$$\frac{d\mathcal{I}_y(0)}{d\mu} = -\frac{e\Delta}{3\pi(\beta+m_0)}, \tag{B18}$$

reproducing Eq. (67).

[1] N. P. Armitage, E. J. Mele, and A. Vishwanath, Rev. Mod. Phys. **90**, 015001 (2018).
[2] B. Yan and C. Felser, Annu. Rev. Condens. Matter Phys. **8**, 337 (2017).
[3] A. A. Burkov, Annu. Rev. Condens. Matter Phys. **9**, 359 (2018).
[4] H. B. Nielsen and M. Ninomiya, Phys. Lett. B **130**, 389 (1983).
[5] D. E. Kharzeev, Prog. Part. Nucl. Phys. **75**, 133 (2014).
[6] A. A. Burkov, J. Phys.: Condens. Matter **27**, 113201 (2015).
[7] J. Xiong, S. K. Kushwaha, T. Liang, J. W. Krizan, M. Hirschberger, W. Wang, R. J. Cava, and N. P. Ong, Science **350**, 413 (2015).
[8] X. Huang, L. Zhao, Y. Long, P. Wang, D. Chen, Z. Yang, H. Liang, M. Xue, H. Weng, Z. Fang, X. Dai, and G. Chen, Phys. Rev. X **5**, 031023 (2015).
[9] R. D. dos Reis, M. O. Ajeesh, N. Kumar, F. Arnold, C. Shekhar, M. Naumann, M. Schmidt, M. Nicklas, and E. Hassinger, New J. Phys. **18**, 085006 (2016).
[10] M. M. Vazifeh and M. Franz, Phys. Rev. Lett. **111**, 027201 (2013).
[11] T. E. O'Brien, C. W. J. Beenakker, and I. Adagideli, Phys. Rev. Lett. **118**, 207701 (2017).
[12] M. J. Pacholski, C. W. Beenakker, and I. Adagideli, Ann. Phys. (NY) **417**, 168103 (2020).
[13] D. Kang, Y. Zhou, W. Yi, C. Yang, J. Guo, Y. Shi, S. Zhang, Z. Wang, C. Zhang, S. Jiang, A. Li, K. Yang, Q. Wu, G. Zhang, L. Sun, and Z. Zhao, Nat. Commun. **6**, 7804 (2015).
[14] Y. Qi, P. G. Naumov, M. N. Ali, C. R. Rajamathi, W. Schnelle, O. Barkalov, M. Hanfland, S.-C. Wu, C. Shekhar, and Y. Sun, Nat. Commun. **7**, 11038 (2016).
[15] L. Zhu, Q.-Y. Li, Y.-Y. Lv, S. Li, X.-Y. Zhu, Z.-Y. Jia, Y. B. Chen, J. Wen, and S.-C. Li, Nano Lett. **18**, 6585 (2018).
[16] S. Cai, E. Emmanouilidou, J. Guo, X. Li, Y. Li, K. Yang, A. Li, Q. Wu, N. Ni, and L. Sun, Phys. Rev. B **99**, 020503(R) (2019).
[17] R. Wang, L. Hao, B. Wang, and C. S. Ting, Phys. Rev. B **93**, 184511 (2016).
[18] M. D. Bachmann, N. Nair, F. Flicker, R. Ilan, T. Meng, N. J. Ghimire, D. Bauer, F. Ronning, J. G. Analytis, P. J. W. Moll, S. Universities, P. Alliance, T. Aviv, and L. Alamos, Sci. Adv. **3**, e1602983 (2017).
[19] O. O. Shvetsov, V. D. Esin, Y. S. Barash, A. V. Timonina, N. N. Kolesnikov, and E. V. Deviatov, Phys. Rev. B **101**, 035304 (2020).
[20] O. O. Shvetsov, Y. S. Barash, S. V. Egorov, A. V. Timonina, N. N. Kolesnikov, and E. V. Deviatov, Europhys. Lett. **132**, 67002 (2020).
[21] K. A. Madsen, E. J. Bergholtz, and P. W. Brouwer, Phys. Rev. B **95**, 064511 (2017).
[22] N. Bovenzi, M. Breitkreiz, P. Baireuther, T. E. O'Brien, J. Tworzydło, I. Adagideli, and C. W. J. Beenakker, Phys. Rev. B **96**, 035437 (2017).
[23] D. Sinha, Phys. Rev. B **102**, 085144 (2020).
[24] P. Dutta, F. Parhizgar, and A. M. Black-Schaffer, Phys. Rev. B **101**, 064514 (2020).
[25] M. Alidoust and K. Halterman, Phys. Rev. B **101**, 035120 (2020).
[26] P. Dutta and A. M. Black-Schaffer, Phys. Rev. B **100**, 104511 (2019).
[27] Y. Kim, M. J. Park, and M. J. Gilbert, Phys. Rev. B **93**, 214511 (2016).
[28] S. Uddin, W. Duan, J. Wang, Z. Ma, and J.-F. Liu, Phys. Rev. B **99**, 045426 (2019).
[29] A. Chen and M. Franz, Phys. Rev. B **93**, 201105(R) (2016).
[30] A. Chen, D. I. Pikulin, and M. Franz, Phys. Rev. B **95**, 174505 (2017).
[31] M. Alidoust, Phys. Rev. B **98**, 245418 (2018).
[32] U. Khanna, D. K. Mukherjee, A. Kundu, and S. Rao, Phys. Rev. B **93**, 121409(R) (2016).
[33] K. Kulikov, D. Sinha, Y. M. Shukrinov, and K. Sengupta, Phys. Rev. B **101**, 075110 (2020).
[34] U. Khanna, S. Rao, and A. Kundu, Phys. Rev. B **95**, 201115(R) (2017).
[35] S.-B. Zhang, J. Erdmenger, and B. Trauzettel, Phys. Rev. Lett. **121**, 226604 (2018).
[36] A. Kononov, G. Abulizi, K. Qu, J. Yan, D. Mandrus, K. Watanabe, T. Taniguchi, and C. Schönenberger, Nano Lett. **20**, 4228 (2020).
[37] Y.-B. Choi, Y. Xie, C.-Z. Chen, J.-H. Park, S.-B. Song, J. Yoon, B. J. Kim, T. Taniguchi, K. Watanabe, H.-J. Lee, J.-H. Kim, K. C. Fong, M. N. Ali, K. T. Law, and G.-H. Lee, Nat. Mater. **19**, 974 (2020).
[38] C. Huang, A. Narayan, E. Zhang, S. Liu, C. Yi, Y. Shi, S. Sanvito, and F. Xiu, Natl. Sci. Rev. **7**, 1468 (2020).
[39] O. O. Shvetsov, A. Kononov, A. V. Timonina, N. N. Kolesnikov, and E. V. Deviatov, JETP Lett. **107**, 774 (2018).

[40] O. O. Shvetsov, A. Kononov, A. V. Timonina, N. N. Kolesnikov, and E. V. Deviatov, Europhys. Lett. **124**, 47003 (2018).
[41] S. Howlader, S. Saha, R. Kumar, V. Nagpal, S. Patnaik, T. Das, and G. Sheet, Phys. Rev. B **102**, 104434 (2020).
[42] S.-B. Zhang, F. Dolcini, D. Breunig, and B. Trauzettel, Phys. Rev. B **97**, 041116(R) (2018).
[43] Y. Liu, Z.-M. Yu, and S. A. Yang, Phys. Rev. B **96**, 121101(R) (2017).
[44] Z. Hou and Q.-F. Sun, Phys. Rev. B **96**, 155305 (2017).
[45] W. Chen, L. Jiang, R. Shen, L. Sheng, B. G. Wang, and D. Y. Xing, Europhys. Lett. **103**, 27006 (2013).
[46] J. Fang, W. Duan, J. Liu, C. Zhang, and Z. Ma, Phys. Rev. B **97**, 165301 (2018).
[47] Z. Faraei and S. A. Jafari, Phys. Rev. B **100**, 035447 (2019).
[48] G. Grabecki, A. Dąbrowski, P. Iwanowski, A. Hruban, B. J. Kowalski, N. Olszowska, J. Kołodziej, M. Chojnacki, K. Dybko, A. Łusakowski, T. Wojtowicz, T. Wojciechowski, R. Jakieła, and A. Wiśniewski, Phys. Rev. B **101**, 085113 (2020).
[49] Y. Naidyuk, O. Kvitnitskaya, D. Bashlakov, S. Aswartham, I. Morozov, I. Chernyavskii, G. Fuchs, S.-L. Drechsler, R. Hühne, K. Nielsch, B. Büchner, and D. Efremov, 2D Mater. **5**, 045014 (2018).
[50] A. Kononov, O. O. Shvetsov, S. V. Egorov, A. V. Timonina, N. N. Kolesnikov, and E. V. Deviatov, Europhys. Lett. **122**, 27004 (2018).
[51] L. Aggarwal, S. Gayen, S. Das, R. Kumar, V. Süß, C. Felser, C. Shekhar, and G. Sheet, Nat. Commun. **8**, 13974 (2017).
[52] D. Breunig, S.-B. Zhang, M. Stehno, and B. Trauzettel, Phys. Rev. B **99**, 174501 (2019).
[53] Y. Liu, Z.-M. Yu, J. Liu, H. Jiang, and S. A. Yang, Phys. Rev. B **98**, 195141 (2018).
[54] X.-S. Li, S.-F. Zhang, X.-R. Sun, and W.-J. Gong, New J. Phys. **20**, 103005 (2018).
[55] H. Li and G. Ouyang, Phys. Rev. B **100**, 085410 (2019).
[56] D. Sinha and K. Sengupta, Phys. Rev. B **99**, 075153 (2019).
[57] S. Mironov and A. Buzdin, Phys. Rev. Lett. **118**, 077001 (2017).
[58] P. Baireuther, J. Tworzydło, M. Breitkreiz, I. Adagideli, and C. W. J. Beenakker, New J. Phys. **19**, 025006 (2017).
[59] M. Z. Hasan and C. L. Kane, Rev. Mod. Phys. **82**, 3045 (2010).
[60] X. L. Qi and S. C. Zhang, Rev. Mod. Phys. **83**, 1057 (2011).
[61] C. W. J. Beenakker, *Mesoscopic Quantum Physics*, edited by E. Akkermans, G. Montambaux, J.-L. Pichard, and J. Zinn-Justin (North-Holland, Amsterdam, 1995), p. 279.
[62] P. W. Brouwer and C. W. Beenakker, Chaos, Solitons Fractals **8**, 1249 (1997).
[63] A. F. Andreev, Zh. Eksp. Teor. Fiz. **46**, 1823 (1964) [Sov. Phys. JETP **19**, 1228 (1964)].
[64] T. Suzuki, R. Chisnell, A. Devarakonda, Y.-T. Liu, W. Feng, D. Xiao, J. W. Lynn, and J. G. Checkelsky, Nat. Phys. **12**, 1119 (2016).